ACS APPLIED MATERIALS & INTERFACES

Research Article

Cite This: ACS Appl. Mater. Interfaces 2018, 10, 33434−33440

www.acsami.org

Black GaAs by Metal-Assisted Chemical Etching

Paola Lova,[†,∥] Valentina Robbiano,[‡] Franco Cacialli,[‡] Davide Comoretto,[§] and Cesare Soci*[,†,∥]

[†]Energy Research Institute at NTU (ERI@N) and Interdisciplinary Graduate School, Nanyang Technological University, 50 Nanyang Avenue, Singapore 639798

[‡]Department of Physics and Astronomy and London Centre for Nanotechnology, University College London, London WC1E 6BT, United Kingdom

[§]Dipartimento di Chimica e Chimica Industriale, Università degli Studi di Genova, via Dodecaneso 31, 16121 Genova, Italy

[∥]School of Physical and Mathematical Sciences, Division of Physics and Applied Physics, Nanyang Technological University, 21 Nanyang Link, Singapore 637371

Supporting Information

ABSTRACT: Large area surface microstructuring is commonly employed to suppress light reflection and enhance light absorption in silicon photovoltaic devices, photodetectors, and image sensors. To date, however, there are no simple means to control the surface roughness of III−V semiconductors by chemical processes similar to the metal-assisted chemical etching of black Si. Here, we demonstrate the anisotropic metal-assisted chemical etching of GaAs wafers exploiting the lower etching rate of the monoatomic Ga<111> and <311> planes. By studying the dependence of this process on different crystal orientations, we propose a qualitative reaction mechanism responsible for the self-limiting anisotropic etching and show that the reflectance of the roughened surface of black GaAs reduces up to ∼50 times compared to polished wafers, nearly doubling its absorption. This method provides a new, simple, and scalable way to enhance light absorption and power conversion efficiency of GaAs solar cells and photodetectors.

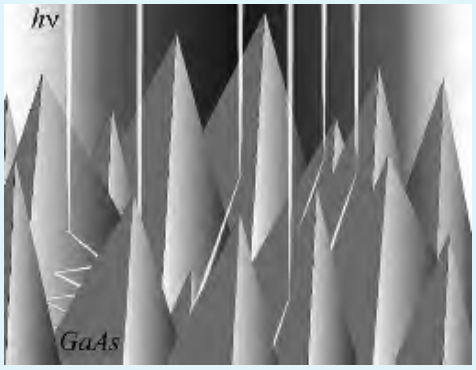

KEYWORDS: *metal-assisted chemical etching, anisotropic etching, perfect antireflection, black GaAs, III−V semiconductors*

INTRODUCTION

Scattering and antireflective superficial layers are widely used to increase the photovoltaic efficiency of inorganic semiconductor,[1,2] conjugated polymer,[3] and perovskite[4,5] solar cells. Such layers rely on light-trapping surfaces,[6,7] scattering structures,[8] and photonic crystals,[9−11] which increase the light path within the photoactive layer, enhance light absorption, and broaden the absorption spectrum.[12] The fabrication of these structures is often accomplished by lithographic techniques, which are hard to implement within the workflow of solar cell production. Wet processes for large-area antireflection or light-trapping surfaces are a low-cost, easily scalable alternative to lithography. For example, metal-assisted chemical etching (MACE) is widely used to fabricate high-aspect-ratio nanowire array with a near-zero surface reflectivity on silicon[13−21] and germanium[22] surfaces. The MACE relies on the dissolution of a substrate operated by a mixture of oxidizing and acidic or alkaline species.[19,23,24] In such processes, a transition metal[13,16,25] catalyses the anisotropic and directional etching of the substrate surface.[24,32,41] As a result, when the catalyst is randomly dispersed on the surface, the process generates nano- and microstructured arrays[14,18,26,27] (see Supporting Information Figure S1 for process details). So far, only few attempts have been made to extend wet etching processes to structure the surface of III−V semiconductors. The MACE of GaAs was demonstrated in conjunction with thermal evaporation,[28] or lithographic patterning of the metal catalyst[29−41] by photolithography,[16] nanoimprint lithography,[42] and microsphere self-assembly,[43] whereas the use of catalyst nanoparticles was shown using Au films evaporated on the GaAs surface and subsequently treated at high temperature.[39] Thermal treatment can induce arsenic vacancies[44] and lead to catalyst diffusion on the GaAs surface. So far, lithographic patterning and thermal evaporation have always been necessary to achieve the desired anisotropic etching of III−V semiconductors, substantially limiting the scalability of the process. Here, we demonstrate a lithography-free MACE process for structuring GaAs surfaces with a near-zero reflection[45] (black GaAs). The method relies on the electroless deposition of randomly dispersed gold nanoparticles cast from solution on the GaAs surface and etching in H_2O_2 and hydrofluoric acid (HF), which are entirely performed in ambient conditions. We find that the antireflective properties of black GaAs outperform those of the well-known micro/nanostructured silicon (black Si), yielding reflectance values as low as 0.013.

Received: June 21, 2018
Accepted: September 7, 2018
Published: September 7, 2018

DOI: 10.1021/acsami.8b10370
ACS Appl. Mater. Interfaces 2018, 10, 33434−33440

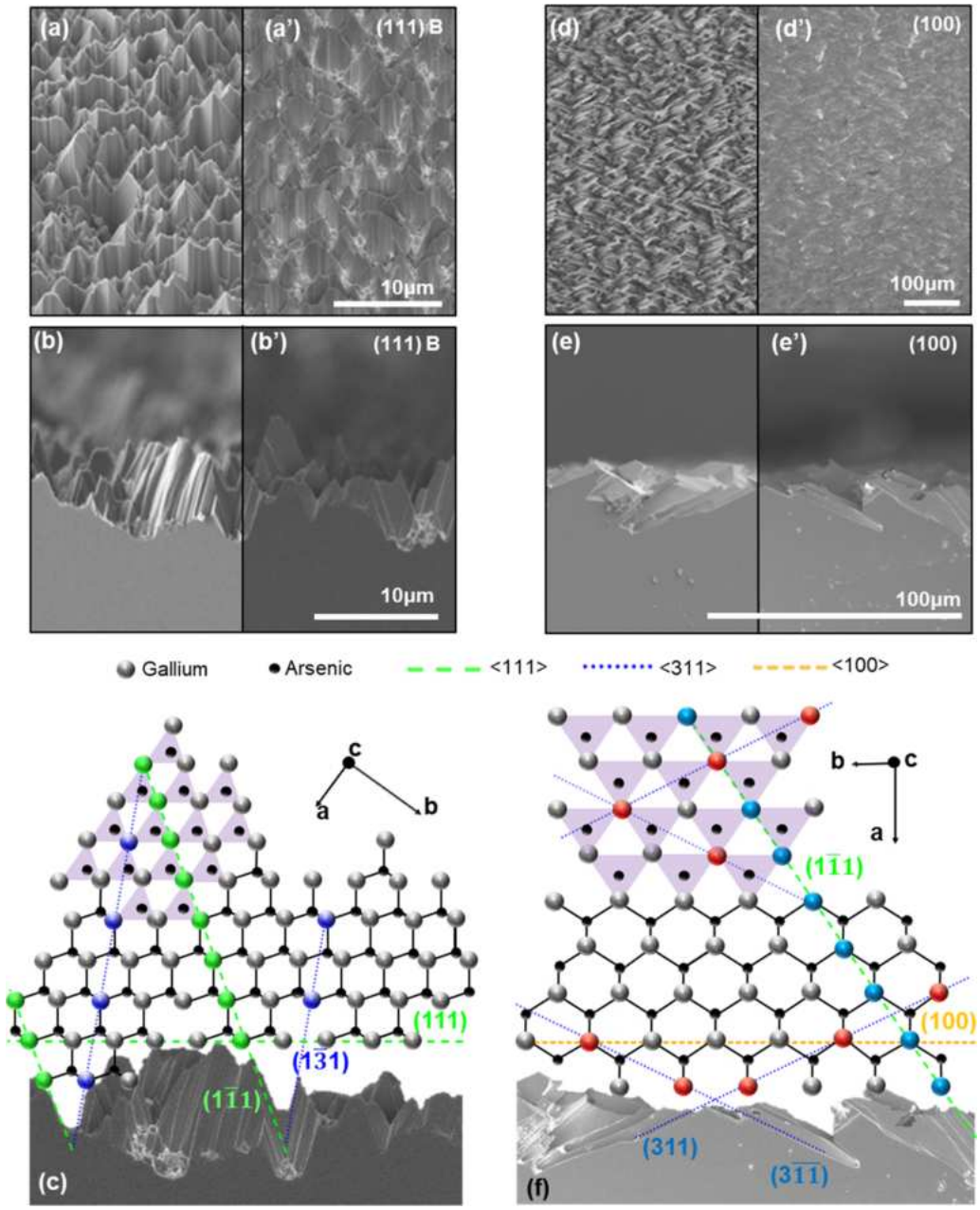

Figure 1. SEM imaging and analysis of the etched (111)B (panels a–c) and (100) (panels d–f) surfaces of GaAs. Top: tilted (a, a′ and d, d′) and cross-sectional views (b, b′ and e, e′) in topographical (a–d) and compositional (a′–d′) modes. Bottom: GaAs crystal representations overlaid to the etched surface profiles (c, f).

EXPERIMENTAL METHODS

Metal-Assisted Chemical Etching. MACE was performed on silicon-doped n-type (111)B, (100), (211), and (110) GaAs epi-ready wafers (purchased from Axt Inc). In a typical process, gold nanoparticles are deposited on the semiconductor surface by immersion in a water solution containing 0.1 mM of $AuCl_3$. The samples are then blow dried and etched in HF/H_2O_2 (4:1) for 10 min.

Reference black Si samples were fabricated by a standard two-step process of p-type (100) Si wafers (purchased from Latech Scientific). First, the samples are etched in a solution of H_2O_2/HF (9:1) containing 0.02 M of $AgNO_3$ for 1 h. Then, further etching in H_2O_2 and NH_4OH (1:3) is carried out to remove residual catalyst and etching byproducts from the surface (see Supporting Information Figure S6).

Structural and Optical Characterization. Microstructure and topography images of the etched surfaces were obtained by scanning electron microscopy (SEM). Data were collected by a field emission SEM Jeol JSM-6700F using acceleration voltage of 5.0 kV and high (SEI) and low (LEI) secondary electrons detectors. Individual SEM images were analyzed to extract the surface features sizes and orientations. Representations of the GaAs crystal lattice were elaborated with the software VESTA[46] using the data retrieved from the Crystallography Open Database.[47]

Reflectance was measured with a spectrophotometer (Andor Shamrock 163i) equipped with an integrating sphere (Bentham IS4-ODM-X) in the spectral range between 550 and 1100 nm. In the 1200–2600 nm spectral range, the data were acquired in a fiber-based optical setup with a Micropak DH2000BAL light source and an Arcoptics FT-interferometer (1000–2600 nm, resolution 8 cm^{-1}).

Photoluminescence external quantum efficiency was measured as previously reported by the method reported by de Mello et al.,[48−50]

DOI: 10.1021/acsami.8b10370
ACS Appl. Mater. Interfaces 2018, 10, 33434−33440

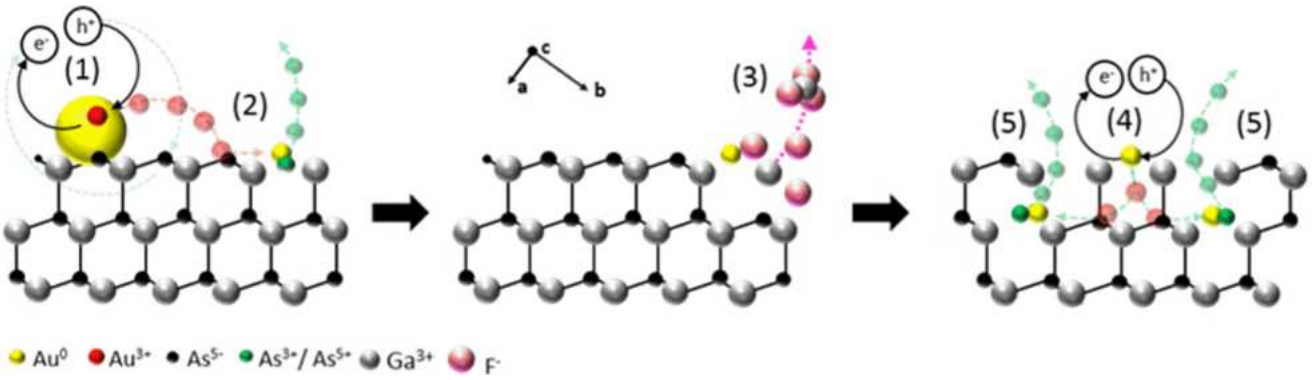

Figure 2. Schematic of the etching process of a (111)B GaAs plane assisted by a gold nanoparticle. (1) Oxidation of the Au nanoparticle by H_2O_2 to form Au ions. (2) Diffusion of Au^{3+} and Au^{1+} ions and oxidation of a reactive As site to produce Au^0 and arsenous and arsenic acids (H_3AsO_3 and H_3AsO_4). (3) Reduction of precipitated Au by H_2O_2 (which becomes available for the oxidation of another reactive site) and complexation of Ga atoms in the (111)A plane by F^- ions allow diffusion of the metal catalyst to the inner surface. (4, 5) Iteration of the process leads to the exposure of the <111> and <311> monoatomic gallium planes.

using an integrating sphere (Avantes AvaSphere-50) coupled to a charge-coupled device (CCD) spectrometer (Avantes 2048) in the 200−1100 nm spectral range. The excitation source was a red diode laser (CNI model MRL-655) with 400 mW power. Wavelength-dependent photoluminescence measurements were performed with a spectrofluorometer (Horiba Fluorolog) equipped with a Si CCD detector. The excitation source was a Xe discharge lamp.

RESULTS AND DISCUSSION

We developed a two-step etching process of GaAs wafers via the electroless deposition of metal nanoparticles (etching catalyst) followed by etching in an acidic oxidizing bath. Randomly dispersed Au nanoparticles are precipitated from an $AuCl_3$ water solution on the GaAs surface by redox reaction between the Au^{3+} ions, which are reduced to Au^0, and GaAs, which is oxidized (see Supporting Information Figure S2). The substrate is then immersed in a bath containing H_2O_2 and HF for 10 min to initiate the catalytic process. Figure 1a,b shows the scanning electron micrographs of the etched GaAs surfaces with the crystallographic orientation (111)B. The topographic images (left side) show the morphology of the surface features, whereas the compositional images (right side) highlight the presence of residual gold nanoparticles, which are also visible as brighter spots in the topographic images.

Etching of the (111)B surface produces randomly oriented, faceted hillocks with heights of about 5.5 μm and width of about 5 μm. It can be immediately noticed that the microfacet orientation remains constant throughout the sample surface, indicating a crystal plane-dependent etching rate. This is further confirmed by the SEM micrographs of the etched wafers with crystal orientations (100), (211), and (110) (see Supporting Information Figures S3 and 1d).

Slow etch rate planes can be identified with the microfacet orientations comparing them with a representation of the GaAs crystal structure (Figure 1c,f). Figure 1c shows that the side facets of the hillocks protruding from the (111)B surface form angles of 70° (blue dotted lines) or 79° (green dashed lines) with the latter, corresponding to the $(1\bar{3}1)$ and $(1\bar{1}1)$ crystallographic orientations. Similarly, the angle between the facets (blue dotted lines in Figure 1f) and the (100) plane (orange lines in Figure 1f) have an angle of 26° with respect to the (100) plane, corresponding to the slow etch rate planes $(3\bar{1}1)$ and $(\bar{1}\bar{1}\bar{1})$.

The fact that monoatomic <111> and <311> planes are etched at slower rate than others can be understood considering the reactivity of individual Ga and As atoms. The sp^3 hybridization of Ga and As atoms in the zinc-blende crystallographic structure of GaAs stabilizes gallium, which is normally trivalent and destabilizes arsenic, which has preferential valence five in electrophilic environment. Because the presence of a lone pair of electrons in As atoms allows their oxidation, a plausible etching mechanism would involve the oxidation of As^{3-} to As^{3+} and As^{5+} to produce arsenous and arsenic acids, whereas fluorine ions withdraw the gallium ions, according to the following reactions

$$GaAs + 3H_2O_2 + 3HF \rightarrow GaF_3 + H_3AsO_3 + 3H_2O \quad (1)$$

$$GaAs + 4H_2O_2 + 3HF \rightarrow GaF_3 + H_3AsO_4 + 4H_2O \quad (2)$$

The reactivity of Ga and As is also linked to the number of bonds that they form with the underlying crystal.[51] When reactive arsenic is etched away from the (111) plane, it reveals a layer of gallium atoms singularly bounded to the crystal, which can be complexed by the fluorine ions. On the other hand, Ga atoms laying on $(1\bar{1}1)$ and $(1\bar{3}1)$ surfaces have respectively two and three bonds with the crystal and are therefore less reactive, slowing down the etch rate (see Supporting Information Figure S4).

Figure 2 shows a schematic of the proposed etching mechanism that accounts for the different reactivity of the species involved. Here, a gold nanoparticle laying on the GaAs (111)B surface is oxidized in an acidic environment by H_2O_2 to form gold ions (1).[52] The resulting Au^{3+} and Au^{1+} ions diffuse along the surface until they encounter a reactive arsenic site and selectively oxidize it to produce Au^0 and arsenous and arsenic acids (2). Whereas the newly precipitated gold is subsequently reduced by H_2O_2 and becomes available for the oxidation of another reactive site, gallium atoms belonging to the (111)A plane can be complexed by the fluorine ions, thus allowing the diffusion of the metal catalyst to the inner surface (3). The process continues until the <111> and <311> monoatomic gallium planes are exposed at the surface (4, 5). To confirm this mechanism, a (111)B GaAs surface was etched without catalyst. In this case, no structure attributable to a plane-dependent etch rate is discernible on the resulting surface (see Supporting Information Figure S5). Note that

DOI: 10.1021/acsami.8b10370
ACS Appl. Mater. Interfaces 2018, 10, 33434−33440

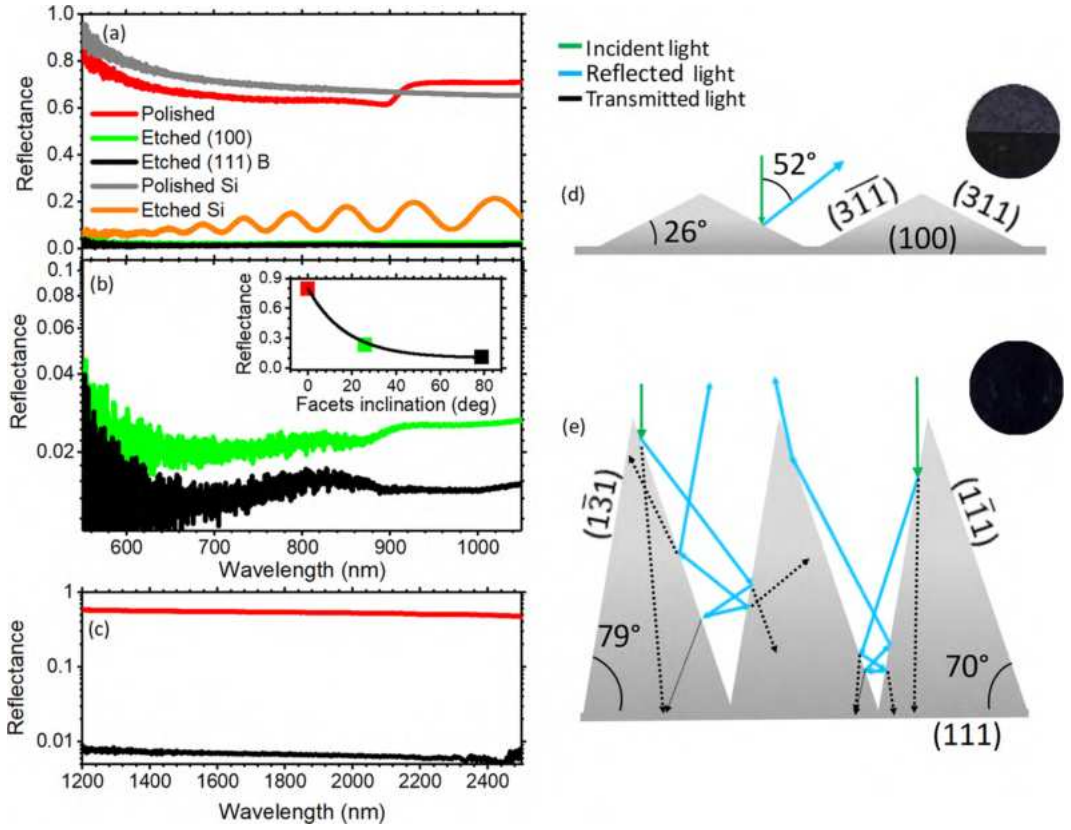

Figure 3. (a) Normal incidence reflectance of polished (red line) and etched (100) (green lines) and (111)B (black lines) GaAs surfaces and polished (gray line) and etched (orange line) Si surfaces. (b) Magnified view of the reflectance spectra of the two GaAs etched surfaces. The inset shows the experimental (squares) and fitted (black line) dependence of the GaAs reflectance collected at 800 nm on the angle of inclination of the faceted surface. (c) Normal incidence reflectance of polished (red line) and etched (111)B (black lines) GaAs surfaces in the near-infrared spectral region. (d, e) Geometrical ray-tracing analysis of the light path within the ideal (100) (c) and (111)B (d) microfaceted surfaces. The insets of (c) and (d) show the overlaid photograph of the etched wafers taken at different collection angles.

previous works that made use of continuous metal film as etching catalyst[33−35,53] could not identify the crystal plane-dependent etching mechanism because gold diffusion to the active sites is inhibited by the catalyst film itself.[32,54]

The etched GaAs samples appear completely black (see the insets of Figure 3c,d), a very desirable property for absorber layers in photovoltaic and photodetection applications. This is due to the nearly perfect suppression of reflectance by the roughened surface, very similar to black Si in which silicon nanowires are formed at the surface by MACE catalyzed by $AgNO_3$ in HF and H_2O_2 (see Experimental Methods section and Supporting Information Figure S6). Figure 3a compares the antireflective properties of black GaAs to those of a reference black Si sample. Compared to polished Si surfaces with reflectance between 0.62 and 0.90 in the range of 550−1150 nm (gray line in Figure 3a), the reflectance of black Si oscillates from a minimum of ∼0.04 to a maximum of ∼0.2, corresponding to a ∼3 to 20-fold reduction. The low surface reflectance of black Si is due to the low refractive index effective medium formed by the nanowire layer, which is also responsible for the pronounced spectral oscillations with typical Fabry−Perot pattern[55] (orange line in Figure 3a). In comparison, the reflectance of black GaAs (black and green lines in Figure 3a) is between ∼25 and 60 times lower than that of polished GaAs (red line in Figure 3a). On average, the antireflective properties of black GaAs are ∼2−10 times better than those of black Si (Supporting Information Figure S7). Note that similar results were also obtained by diffuse reflectance measurements in an integrating sphere (Supporting Information Figure S8). As shown in the following, the nearly perfect antireflection properties of black GaAs stem from a completely different optical mechanism than refractive index matching in black Si.

Figure 3b details the specular reflectance properties of the two types of etched GaAs samples. Although both samples effectively reduce the reflectance of polished GaAs (red line in Figure 3a), both above (absorbing region) and below the band gap at 890 nm (1.4 eV), etched GaAs (111)B has a much lower reflectance than the etched GaAs(100). The lack of an interference pattern in the spectra of the etched GaAs samples suggests that the suppression of reflectance is due to light scattering from the microstructured surface rather the refractive index matching by a surface effective medium like in the case of black Si (see Supporting Information Figure S6). To further confirm this hypothesis, we plotted the reflectance collected at 800 nm as a function of the inclination angle of the faceted surface of the three samples (inset of Figure 3b). The reflectance of the polished surface (0°) is the highest and decreases exponentially with the inclination angle of the facets on the etched surfaces (26° for the (100) and 79° for the (111)B surface, see also Figure 1). This shows that the geometrical light trapping induced by the specific geometry of the surface microfacets of black GaAs is the primary reflection-suppression mechanism. Figure 3c compares the near-infrared reflectance of polished and etched (111)B GaAs surfaces. Whereas polished GaAs is highly reflective and spectrally flat

DOI: 10.1021/acsami.8b10370
ACS Appl. Mater. Interfaces 2018, 10, 33434−33440

throughout the entire near-infrared range (red line), the reflectance of etched GaAs varies between 0.08 at 1200 nm and 0.05 at 2600 nm (black line), corresponding to a 100-fold decrease compared to the polished surface. This makes black GaAs very interesting also for near-infrared photodetector applications.

A simple ray-tracing analysis of the incident light path within the (111)B and (100) etched surfaces provides a qualitative explanation of the light-trapping process (Figure 3d,e). Figure 3d shows an ideal representation of the $(1\bar{1}1)$, $(\bar{1}31)$, and (111) facets on the etched (111)B surface (refer to Figure 1c), whereas Figure 3e depicts the $(3\bar{1}\bar{1})$ and (311) facets on the (100) etched surface (refer to Figure 1f). The microfacets on (100) etched surfaces reflect a normal incident light at ~52°, resulting in strong light scattering and minimal light trapping. Conversely, the $(1\bar{1}1)$ and $(\bar{1}31)$ microfacets on (111)B etched surfaces redirect specularly reflected normal incidence beams toward the bottom of the valleys between facets, which undergo multiple reflections before leaving the surface. Therefore, the larger inclination of surface microfacets explains the superior antireflective characteristics of etched GaAs (111)B compared to (100).

Last, photoluminescence spectra and quantum yield measurements were used to gauge the effectiveness of light trapping in black GaAs. Figure 4 compares the emission spectra of polished GaAs (Figure 4a) and etched GaAs (111)B (Figure 4b) under 559 nm excitation. Both samples show two emission peaks in the near-infrared range, below the band gap. The most intense peak (at 853 and 864 nm in polished and etched GaAs, respectively) is due to the conduction to valence band interband transition (CV),[56,57] whereas the weaker peak (1010 nm in both samples) is assigned to transitions from intragap defect states (IDS), commonly generated from silicon n-type doping.[56,57] The 13 nm (~24 meV) shift of the CV peak and the enhancement of the IDS emission may be ascribed to the formation of new species (e.g., Ga_2O_2 and As_2O_3) on the etched surface, or to the formation of defects and increase of porosity, which are known to cause strain and lattice distortion.[58]

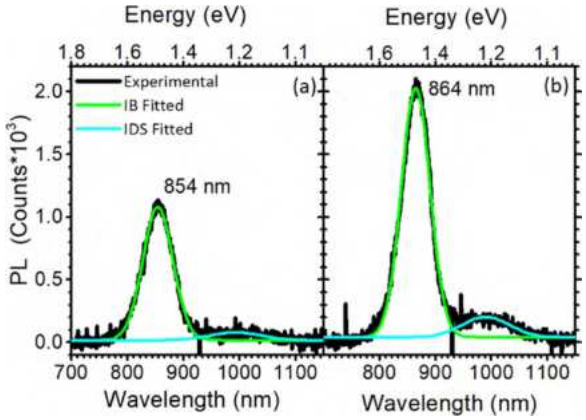

Figure 4. Photoluminescence emission spectra of (a) polished and (b) etched (111)B GaAs samples (black lines). The green and cyan lines are Gaussian fits to the data corresponding to the conduction to valence band (CV) transitions and intragap transitions from defect states (IDS), respectively.

Notably, the photoluminescence intensity of black GaAs is strongly enhanced compared with the polished sample. Whereas the total photoluminescence quantum yield (η_t)[59,60] remains substantially unchanged after etching, the light absorption (Abs) nearly doubles (Table 1, see Experimental Methodssection for measurement details). The increase in light absorption, therefore, largely accounts for the twofold enhancement in integrated emission intensity seen in Figure 4. Interestingly, in the etched sample, the efficiency of the CV transition (η_{cv}) decreases by 20%, whereas the efficiency of the IDS transition (η_{IDS}) is 2.5 times more efficient, yet the total quantum yield remains unaltered. This indicates that, upon absorption, a higher percentage of photoexcitations in black GaAs contribute to the radiative intragap surface defect state transitions than to bulk interband recombination.

CONCLUSIONS

In conclusion, we demonstrated a new metal-assisted chemical etching process to create nearly perfect antireflection microstructured GaAs surfaces in the visible and near-infrared spectral regions (black GaAs). This solution-based process relies on a crystal plane-dependent etch rate, which slows down at monoatomic gallium <111> and <311> crystallographic orientations regardless of the planes exposed to the etchant. Therefore, etching of the (100) or (111)B surfaces generates highly sloped microfacets, which induce efficient light scattering and geometrical light trapping within the semiconductor surface, resulting in up to twofold enhancement in light absorption. We have shown that, on average, the antireflective properties of black GaAs are 2−10 times better than black Si, in which the reduction of surface reflectivity is induced by a refractive index matched surface nanowire layer, rather than by geometrical light trapping. As a result of increased absorption, the intensity of photoluminescence emitted by black GaAs doubles without affecting the external quantum efficiency, even though interband radiative recombination is reduced in favor of the intragap surface defect state transitions. Given its simplicity and scalability, we believe that this method provides a viable way to increase the absorption of III−V semiconductors by microstructuring, and could be readily implemented into the production workflow of solar cells and photodetectors to increase their efficiency.

ASSOCIATED CONTENT

Supporting Information

The Supporting Information is available free of charge on the ACS Publications website at DOI: 10.1021/acsami.8b10370.

Table 1. Absorption (Abs) at 559 nm and Total (η_{tot}), Interband Transition (η_{CV}) and Intraband Surface Defect State Transition (η_{IDS}) Photoluminescence External Quantum Efficiency of Polished and Etched (111)B GaAs

	Abs (λ_{ex} = 559 nm)	η_{tot} (%)	η_{CV} (%)	η_{IDS} (%)
etched	0.9	3.6×10^{-2}	2.6×10^{-2}	1.0×10^{-2}
polished	0.5	3.6×10^{-2}	3.2×10^{-2}	0.4×10^{-2}
ratio (etched/polished)	1.8	1.0	0.8	2.5

DOI: 10.1021/acsami.8b10370
ACS Appl. Mater. Interfaces 2018, 10, 33434−33440

Metal-assisted chemical etching (MACE) process; electroldeless deposition of gold nanoparticles; MACE of (100) and (211) GaAs crystalline planes; slow etching rate planes; noncatalyzed etching of GaAs, black silicon reference; antireflective properties, diffuse reflectance measurements of polished and etched GaAs (PDF)

AUTHOR INFORMATION

Corresponding Author

*E-mail: csoci@ntu.edu.sg.

ORCID

Paola Lova: 0000-0002-5634-6321
Franco Cacialli: 0000-0001-6821-6578
Davide Comoretto: 0000-0002-2168-2851
Cesare Soci: 0000-0002-0149-9128

Author Contributions

The manuscript was written through contributions of all the authors.

Notes

The authors declare no competing financial interest.

ACKNOWLEDGMENTS

The research was supported by the Ministry of Education (MOE2011-T3-1-005, MOE2016-T2-1-052, and MOE2013-T2-1-044) and the National Research Foundation (NRF-CREATE Singapore-Berkeley Research Initiative for Sustainable Energy, SinBeRISE) of Singapore. We also acknowledge support from the European Commission H2020 programme for the ETN SYNCHRONICS funded under grant agreement 643238. F.C. is a recipient of the Royal Society Wolfson Foundation Research Merit Award.

REFERENCES

(1) Savin, H.; Repo, P.; von Gastrow, G.; Ortega, P.; Calle, E.; Garín, M.; Alcubilla, R. Black Silicon Solar Cells with Interdigitated Back-Contacts Achieve 22.1% Efficiency. *Nat. Nanotechnol.* **2015**, *10*, 624−628.

(2) Otto, M.; Algasinger, M.; Branz, H.; Gesemann, B.; Gimpel, T.; Füchsel, K.; Käsebier, T.; Kontermann, S.; Koynov, S.; Li, X.; Naumann, V.; Oh, J.; Sprafke, A. N.; Ziegler, J.; Zilk, M.; Wehrspohn, R. B. Black Silicon Photovoltaics. *Adv. Opt. Mater.* **2015**, *3*, 147−164.

(3) Tang, Z.; Tress, W.; Inganäs, O. Light Trapping in Thin Film Organic Solar Cells. *Mater. Today* **2014**, *17*, 389−396.

(4) Lin, S.-H.; Su, Y.-H.; Cho, H.-W.; Kung, P.-Y.; Liao, W.-P.; Wu, J.-J. Nanophotonic Perovskite Solar Cell Architecture with a Three-Dimensional TiO_2 Nanodendrite Scaffold for Light Trapping and Electron Collection. *J. Mater. Chem. A* **2016**, *4*, 1119−1125.

(5) Du, Q. G.; Shen, G.; John, S. Light-Trapping in Perovskite Solar Cells. *AIP Adv.* **2016**, *6*, No. 065002.

(6) Garnett, E.; Yang, P. Light Trapping in Silicon Nanowire Solar Cells. *Nano Lett.* **2010**, *10*, 1082−1087.

(7) Da, Y.; Xuan, Y.; Li, Q. From Light Trapping to Solar Energy Utilization: A Novel Photovoltaic−Thermoelectric Hybrid System to Fully Utilize Solar Spectrum. *Energy* **2016**, *95*, 200−210.

(8) Brongersma, M. L.; Cui, Y.; Fan, S. Light Management for Photovoltaics Using High-Index Nanostructures. *Nat. Mater.* **2014**, *13*, 451−460.

(9) Leung, S.-F.; Zhang, Q.; Xiu, F.; Yu, D.; Ho, J. C.; Li, D.; Fan, Z. Light management with nanostructures for optoelectronic devices. *J. Phys. Chem. Lett.* **2014**, *5*, 1479−1495.

(10) Lova, P.; Soci, C. Nanoimprint Lithography: Toward Polymer Photonic Crystals. In *Organic and Hybrid Photonic Crystals*; Comoretto, D., Ed.; Springer: Cham, 2015; Chapter 187−212, p 493.

(11) Lova, P.; Cortecchia, D.; Krishnamoorthy, H. N. S.; Giusto, P.; Bastianini, C.; Bruno, A.; Comoretto, D.; Soci, C. Engineering the Emission of Broadband 2D Perovskites by Polymer Distributed Bragg Reflectors. *ACS Photonics* **2018**, *5*, 867−874.

(12) Miller, O. D.; Yablonovitch, E.; Kurtz, S. R. Strong Internal and External Luminescence As Solar Cells Approach the Shockley-Queisser Limit. *IEEE J. Photovoltaics* **2012**, *2*, 303−311.

(13) Li, X.; Bohn, P. W. Metal-Assisted Chemical Etching in HF/H_2O_2 Produces Porous Silicon. *Appl. Phys. Lett.* **2000**, *77*, 2572−2574.

(14) Chartier, C.; Bastide, S.; Lévy-Clément, C. Metal-Assisted Chemical Etching of Silicon in HF−H_2O_2. *Electrochim. Acta* **2008**, *53*, 5509−5516.

(15) Peng, K.; Lu, A.; Zhang, R.; Lee, S.-T. Motility of Metal Nanoparticles in Silicon And Induced Anisotropic Silicon Etching. *Adv. Funct. Mater.* **2008**, *18*, 3026−3035.

(16) Zhang, M.-L.; Peng, K.-Q.; Fan, X.; Jie, J.-S.; Zhang, R.-Q.; Lee, S.-T.; Wong, N.-B. Preparation of Large-Area Uniform Silicon Nanowires Arrays Through Metal-Assisted Chemical Etching. *J. Phys. Chem. C* **2008**, *112*, 4444−4450.

(17) Jansen, H. V.; de Boer, M. J.; Unnikrishnan, S.; Louwerse, M. C.; Elwenspoek, M. C. Black Silicon Method X: A Review on High Speed and Selective Plasma Etching of Silicon with Profile Control: An In-Depth Comparison Between Bosch and Cryostat Drie Processes as a Roadmap to Next Generation Equipment. *J. Micromech. Microeng.* **2009**, *19*, No. 033001.

(18) Srivastava, S. K.; Kumar, D.; Singh, P. K.; Kar, M.; Kumar, V.; Husain, M. Excellent Antireflection Properties of Vertical Silicon Nanowire Arrays. *Sol. Energy Mater. Sol. Cells* **2010**, *94*, 1506−1511.

(19) Huang, Z.; Geyer, N.; Werner, P.; de Boor, J.; Gosele, U. Metal-Assisted Chemical Etching of Silicon: a Review. *Adv. Mater.* **2011**, *23*, 285−308.

(20) Agnieszka, K.; Seán, T. B. Metal-Assisted Chemical Etching Using Sputtered Gold: A Simple Route to Black Silicon. *Sci. Technol. Adv. Mater.* **2011**, *12*, No. 045001.

(21) Smith, Z. R.; Smith, R. L.; Collins, S. D. Mechanism of Nanowire Formation in Metal Assisted Chemical Etching. *Electrochim. Acta* **2013**, *92*, 139−147.

(22) Rezvani, S. J.; Pinto, N.; Boarino, L. Rapid Formation of Single Crystalline Ge Nanowires by Anodic Metal Assisted Etching. *CrystEngComm* **2016**, *18*, 7843−7848.

(23) Elwenspoek, M.; Lindberg, U.; Kok, H.; Smith, L. In *Wet Chemical Etching Mechanism of Silicon*, IEEE Workshop on Micro Electro Mechanical Systems, 1994, MEMS '94, 1994; pp 223−228.

(24) Baca, A. G.; Ashby, C. I. H. *Fabrication of GaAs Devices*; EMIS processing series Bodmin; Institution of Engineering and Technology: U.K., 2005.

(25) Unagami, T. Formation mechanism of porous silicon layer by anodization in HF solution. *J. Electrochem. Soc.* **1980**, *127*, 476−483.

(26) Peng, K.; Xu, Y.; Wu, Y.; Yan, Y.; Lee, S.-T.; Zhu, J. Aligned Single-Crystalline Si Nanowire Arrays for Photovoltaic Applications. *Small* **2005**, *1*, 1062−1067.

(27) Liu, K.; Qu, S.; Zhang, X.; Wang, Z. Anisotropic Characteristics and Morphological Control of Silicon Nanowires Fabricated by Metal-Assisted Chemical Etching. *J. Mater. Sci.* **2013**, *48*, 1755−1762.

(28) Song, Y.; Choi, K.; Jun, D.-H.; Oh, J. Nanostructured GaAs Solar Cells via Metal-Assisted Chemical Etching of Emitter Layers. *Opt. Express* **2017**, *25*, 23862−23872.

(29) Fang, H.; Wu, Y.; Zhao, J.; Zhu, J. Silver Catalysis in the Fabrication of Silicon Nanowire Arrays. *Nanotechnology* **2006**, *17*, 3768.

(30) Yae, S.; Kawamoto, Y.; Tanaka, H.; Fukumoro, N.; Matsuda, H. Formation of Porous Silicon by Metal Particle Enhanced Chemical Etching in HF Solution and its Application for Efficient Solar Cells. *Electrochem. Commun.* **2003**, *5*, 632.

(31) Asoh, H.; Imai, R.; Hashimoto, H. Au-Capped GaAs Nanopillar Arrays Fabricated by Metal-Assisted Chemical Etching. *Nanoscale Res. Lett.* **2017**, *12*, 444.

DOI: 10.1021/acsami.8b10370
ACS Appl. Mater. Interfaces 2018, 10, 33434−33440

(32) Cheung, H.-Y.; Lin, H.; Xiu, F.; Wang, F.; Yip, S.; Ho, J. C.; Wong, C.-Y. Mechanistic Characteristics of Metal-Assisted Chemical Etching in GaAs. *J. Phys. Chem. C* **2014**, *118*, 6903−6908.
(33) Yasukawa, Y.; Asoh, H.; Ono, S. Morphological Control if Periodic GaAs Hole Arrays by Simple Au-Mediated Wet Etching. *J. Electrochem. Soc.* **2012**, *159*, D328−D332.
(34) DeJarld, M.; Shin, J. C.; Chern, W.; Chanda, D.; Balasundaram, K.; Rogers, J. A.; Li, X. Formation of High Aspect Ratio GaAs Nanostructures with Metal-Assisted Chemical Etching. *Nano Lett.* **2011**, *11*, 5259−5263.
(35) Mohseni, P. K.; Kim, S. H.; Zhao, X.; Balasundaram, K.; Kim, J. D.; Pan, L.; Rogers, J. A.; Coleman, J. J.; Li, X. Gaas Pillar Array-Based Light Emitting Diodes Fabricated by Metal-Assisted Chemical Etching. *J. Appl. Phys.* **2013**, *114*, No. 064909.
(36) Asoh, H.; Suzuki, Y.; Ono, S. Metal-Assisted Chemical Etching of GaAs Using Au Catalyst Deposited on The Backside Of A Substrate. *Electrochim. Acta* **2015**, *183*, 8−14.
(37) Lee, A. R.; Kim, J.; Choi, S.-H.; Shin, J. C. Formation of Three-Dimensional GaAs Microstructures by Combination of Wet and Metal-Assisted Chemical Etching. *Phys. Status Solidi RRL* **2014**, *8*, 345−348.
(38) Ono, S.; Kotaka, S.; Asoh, H. Fabrication and Structure Modulation of High-Aspect-Ratio Porous Gaas Through Anisotropic Chemical Etching, Anodic Etching, and Anodic Oxidation. *Electrochim. Acta* **2013**, *110*, 393−401.
(39) Song, Y.; Oh, J. Fabrication of Three-Dimensional GaAs Antireflective Structures by Metal-Assisted Chemical Etching. *Sol. Energy Mater. Sol. Cells* **2016**, *144*, 159−164.
(40) Cowley, A.; Steele, J. A.; Byrne, D.; Vijayaraghavan, R. K.; McNally, P. J. Fabrication and Characterisation of GaAs Nanopillars Using Nanosphere Lithography and Metal Assisted Chemical Etching. *RSC Adv.* **2016**, *6*, 30468−30473.
(41) Kong, L.; Song, Y.; Kim, J. D.; Yu, L.; Wasserman, D.; Chim, W. K.; Chiam, S. Y.; Li, X. Damage-Free Smooth-Sidewall InGaAs Nanopillar Array by Metal-Assisted Chemical Etching. *ACS Nano* **2017**, *11*, 10193−10205.
(42) Glinsner, T.; Kreindl, G. *Lithography*; InTech, 2010, p 656.
(43) Peng, K.; Zhang, M.; Lu, A.; Wong, N.-B.; Zhang, R.; Lee, S.-T. Ordered Silicon Nanowire Arrays via Nanosphere Lithography and Metal-Induced Etching. *Appl. Phys. Lett.* **2007**, *90*, No. 163123.
(44) Birey, H.; Sites, J. Radiative Transitions Induced In Gallium Arsenide by Modest Heat Treatment. *J. Appl. Phys.* **1980**, *51*, 619−624.
(45) Im, K.; Kang, J.-H.; Park, Q. H. Universal Impedance Matching and The Perfect Transmission of White Light. *Nat. Photonics* **2018**, *12*, 143−149.
(46) Momma, K.; Izumi, F. VESTA 3 for Three-Dimensional Visualization of Crystal, Volumetric And Morphology Data. *J. Appl. Crystallogr.* **2011**, *44*, 1272−1276.
(47) http://www.crystallography.net/result.php (retrieved May 21, 2018).
(48) de Mello, J. C.; Wittmann, H. F.; Friend, R. H. An Improved Experimental Determination of External Photoluminescence Quantum Efficiency. *Adv. Mater.* **1997**, *9*, 230−232.
(49) Manfredi, G.; Lova, P.; Di Stasio, F.; Krahne, R.; Comoretto, D. Directional Fluorescence Spectral Narrowing in All-Polymer Microcavities Doped with CdSe/CdS Dot-in-Rod Nanocrystals. *ACS Photonics* **2017**, *4*, 1761−1769.
(50) Lova, P.; Grande, V.; Manfredi, G.; Patrin, M.; Herbst, S.; Würthner, F.; Comoretto, D. All-Polymer Photonic Microcavities Doped with Perylene Bisimide J-Aggregates. *Adv. Opt. Mater.* **2017**, *5*, No. 1700523.
(51) MacFadyen, D. N. On the Preferential Etching of GaAs by H_2SO_4-H_2O_2-H_2O. *J. Electrochem. Soc.* **1983**, *130*, 1934−1941.
(52) Mikhael, B.; Elise, B.; Xavier, M.; Sebastian, S.; Johann, M.; Laetitia, P. New Silicon Architectures by Gold-Assisted Chemical Etching. *ACS Appl. Mater. Interfaces* **2011**, *3*, 3866−3873.
(53) Bienaime, A.; Elie-Caille, C.; Leblois, T. Micro Structuration of GaAs Surface by Wet Etching: Towards a Specific Surface Behavior. *J. Nanosci. Nanotechnol.* **2012**, *12*, 6855−6863.
(54) Song, Y.; Oh, J. Thermally Driven Metal-Assisted Chemical Etching of GaAs with In-Position and Out-Of-Position Catalyst. *J. Mater. Chem. A* **2014**, *2*, 20481−20485.
(55) Sailor, M. J. *Porous Silicon in Practice: Preparation, Characterization and Applications*; John Wiley & Sons, 2012.
(56) Ky, N. H.; Reinhart, F. K. Amphoteric Native Defect Reactions in Si-Doped GaAs. *J. Appl. Phys.* **1998**, *83*, 718−724.
(57) Ha, Y.-K.; Lee, C.; Kim, J.-E.; Park, H. Y.; Kim, S.; Lim, H.; Kim, B.-C.; Lee, H.-C. Defect Luminescence in Heavily Si-Doped n- and p-Type GaAs. *J. Korean Phys. Soc.* **2000**, *36*, 42−48.
(58) Sabataityt, J.; Šimkien, I.; Bendorius, R. A.; Grigoras, K.; Jasutis, V.; Pačebutas, V.; Tvardauskas, H.; Naudžius, K. Morphology and Strongly Enhanced Photoluminescence of Porous GaAs Layers Made by Anodic Etching. *Mater. Sci. Eng., C* **2002**, *19*, 155−159.
(59) Takao, N.; Kyo-ichiro, F.; Taiji, O. Improvement of Quantum Efficiency in Gallium Arsenide Electroluminescent Diodes. *Jpn. J. Appl. Phys.* **1967**, *6*, 665.
(60) Nelson, R. J.; Sobers, R. G. Minority-Carrier Lifetimes and Internal Quantum Efficiency of Surface-Free GaAs. *J. Appl. Phys.* **1978**, *49*, 6103−6108.

DOI: 10.1021/acsami.8b10370
ACS Appl. Mater. Interfaces 2018, 10, 33434−33440